**International Journal of Electrical and Computer Engineering (IJECE)**
Vol. 99, No. 1, Month 2099, pp. 1~1x
ISSN: 2088-8708, DOI: 10.11591/ijece.v99i1.pp1-1x



# Real-time Depth Measurement and Stability Control of AUV using Regression Approximation and Filtered Pressure Data

**Senanjung Prayoga[1], Dhaniel Beny Wardhana [2], Ryan Satria Wijaya[3]**
[1,2,3] Department of Robotics Engineering, Major of Electrical Engineering, Politeknik Negeri Batam, Batam, Indonesia

**Article Info**

***Article history:***

Received month dd, yyyy
Revised month dd, yyyy
Accepted month dd, yyyy

***Keywords:***

Autonomous Underwater Vehicle
Depth Control
PID Controller
Water Pressure Sensor
Sensor Calibration

**ABSTRACT**

This paper presents the development and experimental validation of a prototype-scale autonomous underwater vehicle (AUV) depth control system using a proportional-integral-derivative (PID) controller with depth feedback from a SEN0257 water-pressure sensor. Raw sensor readings are filtered and calibrated using linear regression, reducing the depth estimation error, as indicated by a decrease in RMSE from 1.88 cm to 0.63 cm. The calibrated depth signal is implemented in real time as the feedback source for closed-loop control on the testbed. Controller performance is evaluated by comparing two tuning strategies: Ziegler–Nichols (ZN) closed-loop tuning and manual fine-tuning. Experiments were conducted at depth setpoints of 70 cm and 100 cm under consistent pool conditions, and additional trials were performed while the AUV executes forward motion to assess robustness under dynamic disturbances. System responses are quantified using rise time, overshoot, settling time, and steady-state error. Results show that calibration significantly improves sensor suitability for feedback, while the fine-tuned PID controller produces a more stable depth response with lower overshoot, smaller steady-state error, and shorter settling time than the ZN controller, despite the faster initial rise achieved by ZN tuning. Overall, combining calibrated pressure-based depth estimation with fine-tuned PID gains enables stable and accurate depth regulation for prototype AUV operation.



***Corresponding Author:***

Senanjung Prayoga
Department of Robotics Engineering, Major of Electrical Engineering, Politeknik Negeri Batam, Batam Indonesia
Email: senanjung@polibatam.ac.id

## 1. INTRODUCTION

Autonomous Underwater Vehicles (AUVs) have become crucial assets for tasks such as ocean exploration, subsea infrastructure inspection, and environmental monitoring [1]. In many of these missions, the vehicle must operate at a well-defined depth, making depth regulation a fundamental requirement [2]. In practical implementation, depth is commonly estimated based on hydrostatic pressure using a pressure sensor, which converts the surrounding water pressure into an equivalent depth measurement and provides a straightforward feedback signal for the controller [3]. Nevertheless, maintaining a stable depth under real operating conditions remains challenging, as the vehicle is continuously exposed to disturbances such as waves and currents, as well as strong nonlinear hydrodynamic effects [4].

Despite the wide range of advanced control strategies proposed in the literature, the Proportional-Integral-Derivative (PID) controller remains one of the most widely used solutions for AUV depth regulation due to its conceptual simplicity, modest computational cost, and generally robust performance across operating regimes [5]. Experimental studies indicate that when the gains are carefully tuned, a PID controller can stabilize the vertical motion of an AUV and maintain a desired depth setpoint with small steady-state error, provided that the tuning accounts for the vehicle dynamics and actuator limitations [6][7].

However, in most practical AUV deployments, the performance of the depth control loop still depends heavily on the reliability and accuracy of the pressure sensor, particularly in missions that require precise hovering or steady vertical positioning. Several studies have assessed the accuracy of pressure-based depth measurements against physical reference values; for instance, Duraibabu et al. reported sub-centimeter resolution using a fiber-optic pressure sensor under controlled experimental conditions [8]. Although such results demonstrate high sensor accuracy, fewer studies have experimentally validated pressure-to-depth estimation on an AUV prototype and examined its direct impact on closed-loop depth control performance.

To regulate vertical motion based on pressure-derived depth measurements, the PID controller remains an attractive candidate due to its computational simplicity and widespread deployment. Among various PID tuning strategies, the Ziegler–Nichols (ZN) method is commonly used for rapid, model-free initialization. However, its aggressive gain selection often induces excessive overshoot and oscillatory responses. Consequently, empirical or manual fine-tuning is frequently applied to improve performance under real operating conditions. Kuo et al. employed ZN tuning to obtain initial gains and subsequently performed manual adjustments to reduce overshoot and steady-state error during operation [9]. Nonetheless, a systematic experimental comparison between ZN-tuned and manually fine-tuned PID controllers, evaluated using standard performance metrics on an AUV platform, remains limited in the existing literature.

This study proposes an integrated approach combining sensor calibration and closed-loop PID control to improve both measurement accuracy and depth stability. An experimental AUV testbed is used to validate a hydrostatic pressure-to-depth estimator by comparing sensor-derived depth measurements against ground-truth reference values, thereby demonstrating the effectiveness of pressure sensor calibration in improving depth estimation accuracy. Furthermore, the depth control performance of Ziegler–Nichols tuned and manually fine-tuned PID controllers is rigorously compared using standard time-domain metrics, including rise time, overshoot, settling time, and steady-state error. The robustness of the proposed control approach is also evaluated under realistic operating conditions, including forward motion, to assess its ability to maintain stable depth beyond idealized scenarios. In this context, the study highlights the practical contribution of combining calibrated pressure-based depth estimation with appropriate PID tuning to improve depth stability and control accuracy in prototype AUV applications.

## 2. METHOD

This section describes the research steps needed to achieve the objectives of the AUV depth control system. The process begins with the design of the prototype mechanical structure, the water pressure data acquisition system, and the application of PID control algorithms to maintain depth stability during testing in an aquatic environment.

### 2.1 Mechanical Configuration

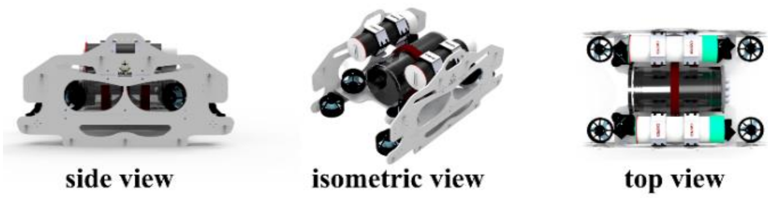


Figure 1. Prototype design of the AUV

Figure 1 shows the mechanical design of the developed AUV prototype. The main structure of the AUV is constructed from a 3 mm thick aluminum plate frame, which is precisely fabricated using laser cutting technology according to the design specifications. The prototype has dimensions of 691 mm in length, 415 mm in width, and 365 mm in height, with an approximate weight of 23 kg. The propulsion system consists of eight thrusters, comprising four horizontal thrusters mounted at a 45° angle to generate forward motion and lateral maneuvering and four vertical thrusters used to regulate depth and directional stability of the AUV. The propulsion units are Blue Robotics T200 thrusters, selected for their high efficiency, strong thrust capability, and reliability in underwater environments [10].

In addition, the AUV prototype is equipped with a ballast system to regulate buoyancy, allowing the vehicle to float and maintain stable positioning in water. The ballast is constructed from a PVC pipe with a diameter of 89 mm and a length of 37 cm, forming a cylindrical structure that provides stable buoyancy during underwater operation [11].

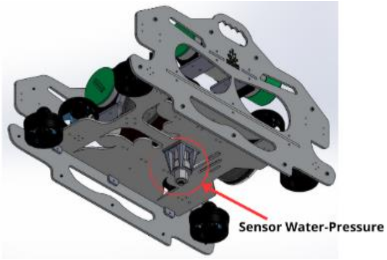


Figure 2. Placement of the SEN0257 pressure sensor

The water pressure sensor is installed at the bottom center of the AUV frame, as shown in Figure 2. This position was chosen because it is at the vehicle's vertical balance point, allowing the sensor to detect water pressure directly when the bottom of the AUV begins to touch the water surface [12]. This central placement ensures more accurate and stable measurement results, unaffected by waves or currents around the body. In addition, this position also maintains the hydrodynamic symmetry of the AUV and helps the control system obtain more responsive and consistent depth data during testing.

## 2.2 AUV Pressure Sensor System

The dataset used in this study is obtained from real measurements of a water pressure sensor installed on the AUV prototype. The pressure data are acquired directly from the SEN0257 water pressure sensor, which measures hydrostatic pressure and provides Analog output proportional to the surrounding water depth. The sensor output is sampled using the Analog-to-Digital Converter (ADC) of the STM32F103C8T6 microcontroller during experimental tests conducted under both static conditions and forward-motion operation of the AUV. The collected pressure data are used as the primary input for depth estimation and feedback control in the PID-based depth control system.

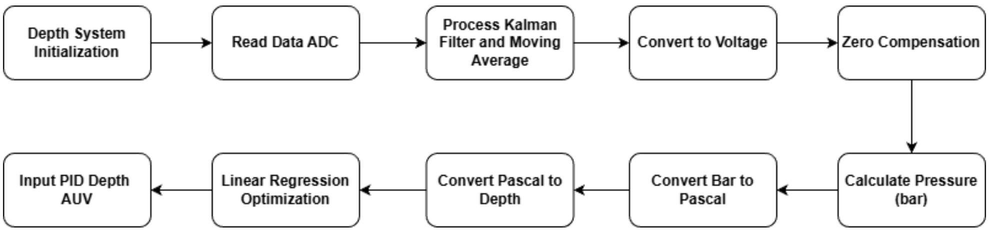


Figure 3. Block diagram of the water pressure signal processing system for the AUV

Figure 3 illustrates the block diagram of the water pressure reading system used to estimate the depth of the AUV. Data from the pressure sensor are processed sequentially, starting from raw signal readings to producing the final depth value used as the main input to the depth control system (PID).

In the initial stage, the system acquires Analog-to-Digital Converter (ADC) output from the pressure sensor. Since the raw ADC signal is affected by noise originating from the sensor and the aquatic environment, a two-stage filtering approach is applied to improve signal stability. In the first stage, a Kalman filter is employed to recursively estimate the true ADC value by combining the current measurement with the previous state estimate while accounting for estimation uncertainty. The filtering process involves the calculation of the Kalman gain, followed by updating the state estimate and the error covariance, as defined in Equation (1).

$$K_k = \frac{Q_{k-1}}{Q_{k-1}+R} \quad (1)$$

$$X_k = X_{k-1} + K_k(Z_k - X_{k-1})$$

$$Q_k = (1 - K_k)Q_{k-1}$$

In Equation (1), $Z_k$ denotes the ADC measurement at time step $k$, $X_k$ is the Kalman filtered ADC estimate, $Q_k$ is the estimation error covariance, and $R$ = 30.0 is the measurement noise variance representing sensor uncertainty. The process noise is set to $Q$ = 0.01, with initial conditions $X_0 = 0$ and $Q_0 = 1.0$, used as the starting point for the first iteration of the Kalman filter, where $X_0$ provides the initial estimate of the ADC value and $Q_0$ represents the initial uncertainty of this estimate. These values were chosen to balance filter responsiveness and noise suppression [13]. After Kalman filtering, an additional smoothing stage is applied using a moving average filter to further reduce residual signal fluctuations [14]. The smoothing process is defined in Equation (2).

$$\overline{\{X_n\}} = \frac{1}{M}\ \sum_{i=0}^{M-1} X_{n-i} \tag{2}$$

This filter calculates the average of the last $M$ samples, where $M = 23$ is used in this study. This process produces a smoother and more stable signal that is less sensitive to small variations in the aquatic environment [15]. After the filtering process is completed, the stabilized ADC value is converted into a voltage using the ADC conversion relationship expressed in (3), where $N_{adc}$ is the measured ADC value, $\mathrm{N}_{\mathrm{ma}_\mathrm{x}}$ is the maximum ADC resolution, and is the reference voltage.

$$V_{meas} = \frac{N_{adc}}{\mathrm{N}_{\mathrm{ma}_\mathrm{x}}}\ \times \mathrm{V}_{\mathrm{ref}} \tag{3}$$

Where $N_{adc}$ is the measured ADC value, $\mathrm{N}_{\mathrm{ma}_\mathrm{x}}$ is the maximum ADC resolution, and $V_{ref}$ is the ADC reference voltage. The measured voltage is then corrected to eliminate the water surface offset in order to obtain the corrected voltage in Equation (4).

$$V_{corr} = V_{meas} - V_{offset} \tag{4}$$

The voltage $V_{offset}$ represents the baseline voltage measured when the sensor is located at the water surface. Based on the corrected voltage, the water pressure is calculated in bar units using the sensor sensitivity, as expressed in (5). The parameter $V_{per\_bar}$ indicates the voltage change corresponding to one bar of pressure. The resulting pressure value is then converted into Pascal units using Equation (6).

$$P_{bar} = \frac{Vcorr}{V_{per\_bar}} \tag{5}$$

$$P_{pa} = P_{bar}\ x\ 100000 \tag{6}$$

Subsequently, the hydrostatic pressure is converted into depth using the hydrostatic relationship Equation (7). Where $\rho$ denotes the water density and $g$ represents the gravitational acceleration. The resulting depth in meters is then converted into centimeters using Equation (8).

$$H_m = \frac{P_{pa}}{\rho g} \tag{7}$$

$$h_{cm} = 100\ x\ H_m \tag{8}$$

The value of $h_{cm}$ represents the ideal depth obtained from the physical pressure-to-depth conversion. To compensate for systematic errors introduced by the pressure sensor and signal conditioning circuitry, a signal-variable linear regression calibration model is applied, as expressed in (9).

$$y = mx + c \tag{9}$$

In this study, $h_{cm}$ is defined as the raw depth obtained from the physical pressure-to-depth conversion, while $h_{cm\_cal}$ represents the calibrated depth produced by applying the linear regression model. The calibration relationship is expressed in Equation (10), where $m$ and $c$ represent the slope and intercept of the calibration curve, respectively, and are determined experimentally during the calibration process. The slope represents sensor sensitivity, while the intercept reflects the baseline offset, enabling compensation of systematic errors and improved depth estimation accuracy.

$$h_{cm\_cal} = m\ \cdot h_{cm} + c \tag{10}$$

The value $h_{cm\_cal}$ is the calibrated depth in centimeters used as an estimate of the final depth of the AUV in the water. The result of this calculation then becomes an important input for the AUV depth PID control system to ensure that the AUV can maintain the depth according to the specified setpoint.

### 2.3 Depth Measurements Method Scheme of an AUV Using a Pressure Sensor

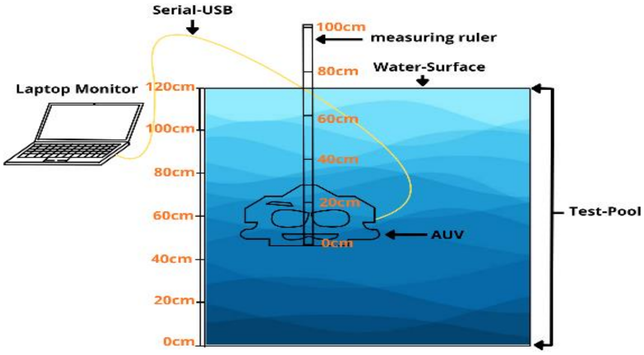


Figure 4. Illustrations of pressure data collection for AUV depth estimation

Figure 4 shows the test configuration and workflow of the water pressure reading system for estimating the depth of the AUV. In this test, the AUV was placed in a test pool at several target depths. A measuring ruler is attached to the robot body with the bottom of the ruler parallel to the bottom of the AUV frame body. This configuration enables direct measurement of the actual depth using a reference scale. The pressure sensor reads the hydrostatic pressure according to the depth, and then the data is processed by a microcontroller and sent to a laptop via Serial-USB to be displayed as the estimated depth. The estimated depth value is compared with the actual depth to calculate the error and assess repeatability. Furthermore, the measurement data is used to form a calibration model through linear regression using equation (9), so that the estimated depth can be corrected and its accuracy re-evaluated. This linear regression-based calibration approach, supported by a data filtering process, is commonly applied in pressure sensor-based AUV depth systems to improve the quality and stability of estimated data [16][17].

### 2.4 PID Control System AUV

This subsection describes the depth control system implemented on the AUV. First a block diagram of the overall system is presented, followed by the PID-based depth control structure, and finally the gain tuning procedure using the Ziegler-Nichols method and manual fine-tuning [18].

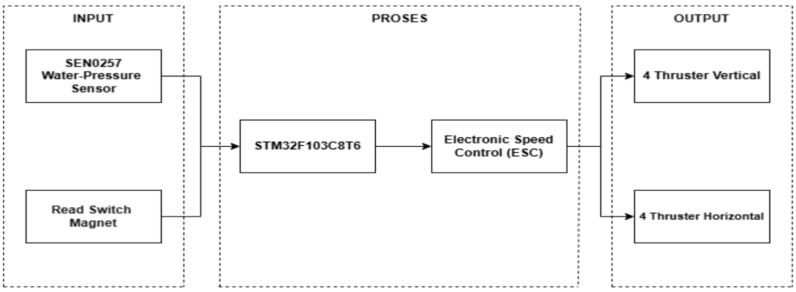


Figure 5. Block diagram system AUV

Figure 5 shows a block diagram of the system used in this study. The system consists of three main components, namely the SEN0257 water pressure sensor, which is used to measure hydrostatic pressure around the AUV, and a magnetic read switch that functions as a control switch. The read switch is used to activate the control mode.

The STM32F103C8T6 microcontroller acts as the data processing center by reading signals from pressure sensors. Based on the depth data, the microcontroller implements a PID-based depth control algorithm to generate the appropriate control signals [19].

Control signals from the microcontroller are sent to the electronic speed controller (ESC), which then regulates the speed of four vertical thrusters as actuators on the Z-axis and four horizontal thrusters to move forward. Coordination between the ESC and these thrusters allows the AUV to generate downward thrust and move forward in a controlled manner, enabling the vehicle to maintain or reach the desired depth and maneuver forward in a stable and precise manner.

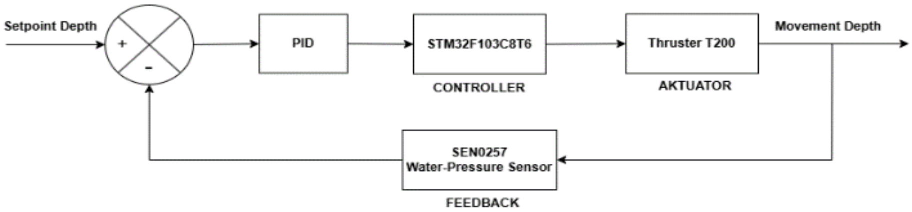


Figure 6. Block diagram control AUV

Figure 6 shows a block diagram of the depth control system used in the AUV prototype. The input signal is the depth setpoint reference. When the AUV has not yet reached that depth, an error difference arises between the reference value and the achieved depth. This error value is then processed by the PID controller to produce a control signal that regulates the thruster so that the AUV can approach and maintain the setpoint depth [20][21]. The measured depth value is sent back as a feedback signal to the summing block so that the closed control loop can work continuously.

In practical implementation, the PID controller output is applied to the AUV thrusters via the electronic speed controller (ESC). To avoid actuator saturation, the control signal is limited to a pulse-width modulation (PWM) range of -200 to 300, which represents the minimum and maximum allowable commands for the vertical thrusters. When the control signal reaches these limits, further increases in control effort no longer affect the actuator response.

To prevent integral windup under saturation conditions, an anti-windup mechanism based on integral clamping is implemented. The integral term accumulation is suspended whenever the control output reaches the predefined PWM bounds, preventing excessive integral growth when the AUV has not yet reached the depth setpoint. This method reduces overshoot, improves stability near the setpoint, and enhances the robustness of the depth control system during large depth errors and transient conditions.

## 2.5 PID tuning using Ziegler-Nichols

Proportional Integral Derivative (PID) controllers are used to regulate system response based on the difference between the setpoint value and the system output. The PID controller consists of three main components, namely Proportional (P), Integral (I), and derivative (D), which function to accelerate system response, reduce steady-state error, and improve response stability [22][23].

PID parameter tuning is performed using the Ziegler-Nichols closed-loop method to obtain the initial controller parameters. The tuning process begins by deactivating the integral and derivative actions, by settling $K_i$ = 0 and $K_d$ = 0, so that the system is only controlled by the proportional action ($K_p$) and then gradually increased until the system response shows continuous oscillation with a relatively constant amplitude. This condition indicates that the system is at the boundary between stability and instability. The $K_p$ value in this condition is defined as the ultimate gain ($K_u$). The oscillation period $K_p = K_u$ is measured as the ultimate period ($P_u$). This is the time difference between two consecutive oscillation peaks. The $K_u$ and $P_u$ values are used as the basis for calculating the initial control parameters based on the Ziegler-Nichols rule [24].

Table 1. Ziegler-Nichols formula in gain form

| Controller | $K_p$ | $K_i$ | $K_d$ |
|---|---|---|---|
| P | $0.5K_u$ | 0 | 0 |
| PI | $0.45K_u$ | $\frac{1.2K_p}{P_u}$ | 0 |
| PID | $0.6K_u$ | $\frac{2K_p}{P_u}$ | $\frac{K_pP_u}{8}$ |

Table 1 shows the Ziegler-Nichols closed-loop tuning rules used to determine the initial controller gains based on the measured ultimate gain ($K_u$) and ultimate period ($P_u$). The P controller applies only proportional action with $K_p = 0.5K_u$, while $K_i$ and $K_d$ are set to zero. The PI controller sets $K_p = 0.45K_u$ and introduces integral action using $K_i = \frac{1.2K_p}{P_u}$ to reduce steady-state error. The PID controller computes the initial gain as $K_p = 0.6K_u$, $K_i = \frac{2K_p}{P_u}$ , and $K_d = \frac{K_pP_u}{8}$ to provide a faster and more stable response as a starting point before fine tuning.

### 2.6 PID Fine Tuning Using Manual Trial and Error

The PID fine-tuning method with a manual trial-and-error approach is performed directly on the system without requiring a mathematical model of the plant. Tuning is performed by gradually changing the PID parameter values, then assessing the system response through response graphs, such as rise time, overshoot, settling time, and steady-state error [25][26].

Table 2. Determination of fine tuning parameters

| Parameter | Rise time | Overshoot | Settling time | Steady state error |
|---|---|---|---|---|
| $K_p$ | Down | Go Up | Minor Changes | Down |
| $K_i$ | Down | Go Up | Go Up | Removed |
| $K_d$ | Minor Change | Down | Down | Minor Changes |

As shown in Table 2, increasing $K_p$ generally reduces rise time and steady-state error, but tends to increase overshoot, while its effect on settling time is relatively small. Increasing $K_i$ can reduce or eliminate steady-state error and can shorten rise time however, it typically increases overshoot and lengthens settling time if set too high. Conversely, increasing $K_d$ primarily increases damping by reducing overshoot and settling time, with only minor changes to rise time and steady-state error. Therefore, during fine-tuning, $K_p$ is adjust to speed up the response, $K_i$ is carefully increased to eliminate steady-state error, and $K_d$ is set to suppress oscillations and improve stability around the setpoint.

## 3. RESULTS AND DISCUSSION

### 3.1. Optimized Sensor Water-Pressure

This test was conducted to evaluate the accuracy of the water pressure sensor-based depth measurement system used in the AUV. The pressure signal is read by a microcontroller, then converted into a depth estimate and sent to a computer to be displayed on the monitor interface.

In this static test, the system was tested at five reference depths, namely 20, 40, 60, 80, and 100 cm. At each depth, four measurements were taken to evaluate the repeatability of the sensor readings and identify measurement biases in the operating range. The actual depth was measured using a ruler made from a 120 cm long PVC pipe marked with distances using a tape measure so that it could function as a reference measuring tool. The actual depth values were then compared with the depth values displayed on the monitor as the output of the water pressure sensor system.

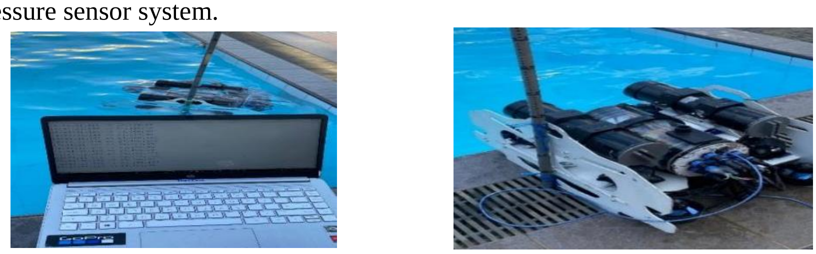

(a) Depth prediction on the monitor (b) Actual depth measurements

Figure 7. Comparison between the depth predicted by the water pressure sensor system (a) and the actual depth measured manually (b).

Figure 7 presents a comparison between the predicted and actual depth values. Figure 7(a) shows the depth values predicted by the system and displayed on the monitor laptop, while Figure 7(b) shows the actual depth measured using a ruler. The values displayed on the monitor represent the results of water pressure signal processing by the microcontroller, whereas the actual depth is used as a reference to evaluate the accuracy of the measurement system.

Table 3. Pressure sensor data before regression

| Depth Actual (cm) | Test 1 | Test 2 | Test 3 | Test 4 | Mean Raw Reading (cm) | Error (cm) |
|---|---|---|---|---|---|---|
| 20 | 22 | 21 | 21 | 20 | 21.00 | 1.00 |
| 40 | 43 | 42 | 43 | 43 | 42.75 | 2.75 |
| 60 | 60 | 61 | 61 | 62 | 61.00 | 1.00 |
| 80 | 81 | 81 | 80 | 81 | 80.75 | 0.75 |
| 100 | 103 | 103 | 104 | 101 | 102.75 | 2.75 |
| RMSE | | | | | | 1.88 |

Table 3 shows the water pressure sensor data before linear regression was performed at five reference depths. At each depth, four measurements were taken, and then the average sensor reading, mean raw reading, and the error value in centimeters were calculated. In the error column (cm), the error is defined as the absolute value of the difference between the average depth of the sensor reading and the actual depth at each test point. Table 3 shows that at all test points, the mean raw reading value was always slightly greater than the actual depth, so the sensor tended to overestimate the depth, especially at 40 cm and 100 cm with errors of 2.75 cm, respectively. Overall, the root mean square error RMSE value for the data before regression is 1.88 cm, which indicates that the raw pressure sensor data is not accurate enough to be used directly as depth feedback. The RMSE value is calculated using Equation (11).

$$RMSE = \sqrt{\frac{1}{n}\sum_{i=1}^{n} e_i^2} \qquad (11)$$

Where $ei$ represents the difference between the average depth reading from the sensor and the actual depth at test point $i$, and $n$ is the number of depth points tested (in this study, $n$ = 5). During the optimization stage, the relationship between the pressure sensor output and the actual depth was modeled using linear regression. In this modeling, the pressure sensor reading $x$, which was still in the form of raw depth (un-calibrated and still containing offset), was treated as an independent variable, while the actual depth $y$ was used as a reference value. The calibration relationship between the two is expressed in the equation (12).

$$yz = mx + c \qquad (12)$$

Where $xi$ is the pressure sensor reading (cm) at the $i$-th sample, $yi$ is the actual depth (cm) at the $i$-th sample, and $yz$ is the calibrated depth (cm). The linear regression parameters, namely the slope $m$ and intercept $c$, are obtained using the least squares method. Specifically, the slope $m$ is computed using Equation (13), while the intercept $c$ is calculated using Equations (14).

$$m = \frac{n\sum_{i=1}^{n}(x_i y_i) - (\sum_{i=1}^{n} x_i)(\sum_{i=1}^{n} y_i)}{n\sum_{i=1}^{n} x_i^2 - (\sum_{i-1}^{n} x_i)} \qquad (13)$$

$$c = \frac{\sum_{i=1}^{n} y_i - m\sum_{i=1}^{n} x_i}{n} \qquad (14)$$

Based on all calibration data consisting of $n$ = 20 samples (5 depth with 4 repetitions), calculations using equations (13) and (14) produced a slope value $m$ of 0.991 and a constant $c$ of -1.095. Thus, the water pressure sensor calibration model used in this study is stated as follows:

$$y_Z = 0.991_x - 1.095 \qquad (15)$$

Based on Equation (15), $x$ represents the raw sensor reading prior to calibration (in centimeters), while $y_z$ denotes the calibrated depth value expressed in centimeters. This calibration equation is applied to correct systematic measurement errors and improve the accuracy of depth estimation obtained from the sensor.

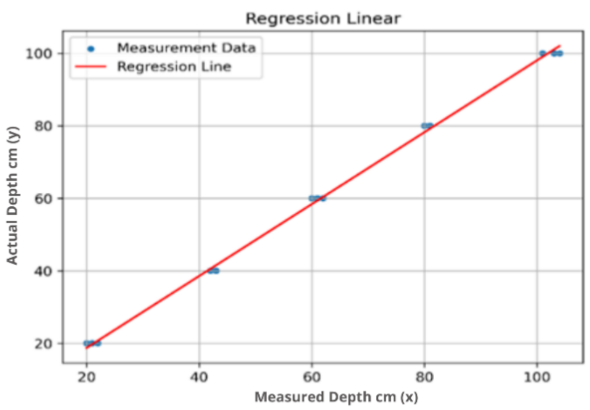

Figure 8. Optimization chart linear regression

Figure 8 shows the distribution of measurements data from the linear regression line obtained. In this graph, the x-axis represents the pressure sensor readings, while the y-axis represents the actual depth. The measurements points appear to coincide with the regression line, indicating that the linear model provides an excellent approximation of the calibration data.

Table 4. Pressure sensor data after regression

| Depth Actual (cm) | Optimized Water pressure | Error |
|---|---|---|
| 20 | 20 | 0 |
| 40 | 40 | 0 |
| 60 | 59 | 1 |
| 80 | 79 | 1 |
| 100 | 100 | 0 |
| RMSE | | 0.63 |

Table 4 shows the performance of the pressure sensor after calibration using linear. The Optimized Water-Pressure value is the depth of calibration and actual depth. The maximum error is only about 1 cm at depth 60 cm and 80 cm, while at depths of 20 cm, 40 cm, and 100 cm, the error is zero. Overall, the RMSE value decreased to 0.63 cm, indicating that the calibration results significantly improved the accuracy of depth measurements compared to the conditions before regression.

### 3.2. Comparison of Fine Tuning PID Control and Ziegler-Nichols at a Setpoint of 70 cm

This experiment aims to compare the performance of two sets of PID parameters at a depth setpoint of 70 cm, namely the manually fine-tuned PID parameters and the PID parameters obtained using the Ziegler–Nichols method. All experiments were conducted under identical test pool conditions using a water pressure sensor as depth feedback, ensuring a consistent and fair performance comparison between the two control strategies. The Ziegler-Nichols parameters are determined through closed-loop testing by disabling integral and derivative action ($K_i$ = 0, $K_d$ = 0), then gradually increasing $K_p$ until the system exhibits continuous oscillation with a relatively constant amplitude. In the test, stable oscillations were obtained at $K_p$ = 4.2667 so $K_u$ = 4.2667 was set.

The $P_u$ value is obtained from the time difference between two consecutive oscillations peaks (peak-to -peak) when $K_p = K_u$. Based on the oscillation graph, $P_u$ = 11.24 is obtained. These $K_u$ and $P_u$ values are used to calculate the initial PID parameters based on the Ziegler-Nichols rule. Subsequently, the PID parameters were further refined through manual fine-tuning. This process involved adjusting the controller gains based on the observed system response in order to reduce oscillations and minimize steady-state error around the 70 cm depth setpoint. The PID parameters obtained from both methods are summarized in Table 5 and Table 6.

Table 5. Ziegler-Nichols method parameters

| Parameter | Value |
|---|---|
| $K_p$ | 2.560 |
| $K_i$ | 0.455 |
| $K_d$ | 3.596 |

Table 5 presents the PID parameters determined using the Ziegler-Nichols tuning method. The proportional gain $K_p$ = 2.560 provides a fast initial response to depth errors. The integral gain $K_i$ = 0.455 is relatively low, while the derivative gain $K_d$ = 3.596 is considerably high. This configuration reflects the aggressive nature of the Ziegler-Nichols method, which is designed to achieve rapid system response but may result in larger oscillations around the setpoint.

Table 6. Fine-Tuning method parameters

| Parameter | Value |
|---|---|
| $K_p$ | 2.560 |
| $K_i$ | 0.635 |
| $K_d$ | 0.052 |

Table 6 shows the PID parameters obtained through manual fine-tuning based on the initial Ziegler-Nichols parameters. The proportional gain $K_p$ was maintained to preserve response speed, while the integral gain $K_i$ was increased to 0.635 to further reduce steady-state error. The derivative gain $K_d$ was significantly reduced to 0.052, indicating that derivative action is primarily used to smooth the system response and suppress minor oscillations. Overall, this tuning configuration prioritizes stability and accuracy of depth control around the desired setpoint.

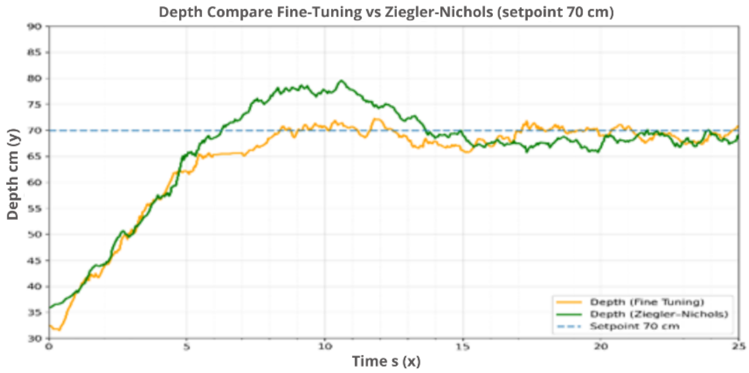

Figure 9. Graph 70 cm depth response fine tuning vs Ziegler-Nichols

Figure 9 shows that the fine-tuned PID controller produces a relatively slower but stable response. At a setpoint of 70 cm, a rise time of approximately 6.2 s and a settling time of approximately 15.35 s are obtained. Overshoot and steady-state error calculations are performed using Equations (16) and (17) as follows:

$$Overshoot = \frac{Max\ Response - Setpoint}{Setpoint} x\ 100\% \quad (16)$$

$$Error\ ss = \frac{Setpoint - Steady\ State}{Setpoint} x\ 100\% \quad (17)$$

In Equation (16), the maximum response (Max Response) refers to the peak output value after the setpoint is applied, while in Equation (17), the steady-state (Steady State) represents the output value when the system reaches equilibrium. Based on the 70 cm setpoint test data, the PID fine-tuning method produced a rise time of 6.2 s, a settling time of 15.35 s, a maximum response of 70.77 cm, and a steady-state value of 69.77 cm. Referring to Equations (16) and (17), the overshoot and steady-state error were 0.33% and 1.1%, respectively. For the Ziegler–Nichols PID method, the system produced a rise time of 5 s, a settling time of 20.1 s, a maximum response of 80 cm, and a steady-state value of 68.5 cm. Based on Equations (16) and (17), the overshoot and steady-state error were 14.29% and 2.14%, respectively.

These results indicate that the fine-tuning method provides a more stable and accurate response around the 70 cm setpoint, as it results in a shorter settling time and lower overshoot and steady-state error compared to the Ziegler–Nichols method.

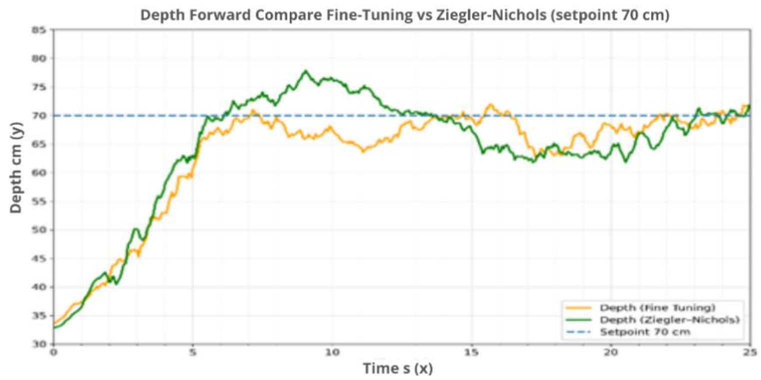

Figure 10. Graph 70 cm depth response fine tuning vs Ziegler-Nichols depth forward

Figure 10 shows the depth response of the AUV during forward motion for two sets of PID fine-tuning parameters and the Ziegler–Nichols method. The Ziegler–Nichols controller provides a faster initial response but is more aggressive, resulting in greater overshoot. Based on the test results, the maximum response reached 77.7 cm, the steady-state value was 68.3 cm, the rise time was 4.2 s, and the settling time was 21.8 s. Referring to Equations (16) and (17), the overshoot and steady-state error were 11% and 2.4%, respectively. These values indicate that the Ziegler–Nichols controller provides a fast initial response but produces higher overshoot and a larger steady-state error, resulting in poorer depth stability around the 70 cm setpoint during forward motion.

The fine-tuned PID controller exhibits smoother response characteristics. At a setpoint of 70 cm, a rise time of 5.2 s and a settling time of 19.6 s were obtained. Based on the test data, the maximum response reached 71.5 cm and the steady-state value was 69.2 cm. Referring to Equations (16) and (17), the overshoot and steady-state error were 2.14% and 1.1%, respectively. These results indicate that the fine-tuning method produces lower overshoot and smaller steady-state error compared to the Ziegler–Nichols method, thereby improving depth stability during forward motion.

### 3.3. Results of the AUV Prototype Depth Control Test at a Setpoint of 100 cm

The next test was conducted by setting the AUV prototype to reach a depth of 100 cm using a PID controller that had been adjusted according to the control parameters listed in Table 6. At the beginning of the test, the AUV was at a depth of approximately 32 cm, and then it moved downward following the setpoint command until it reached a depth of 100 cm. The condition of the AUV prototype at a depth of 100 cm is shown in Figure 11, illustrating that the vehicle successfully reaches and maintains the desired depth.

Figure 11. AUV position at a depth of 100 cm

The depth response of the AUV toward the 100 cm setpoint using the fine-tuned PID controller is shown in Figure 12, which illustrates the dynamic behavior of the system during the depth control process.

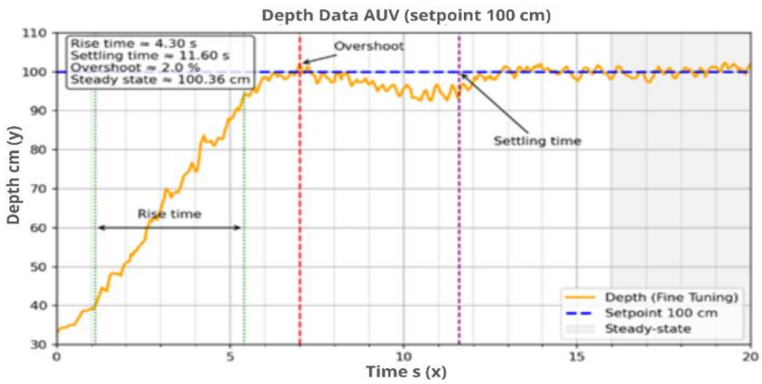


Figure 12. Depth response at the 100 cm setpoint using the fine-tuned PID controller

Based on Figure 12, the main characteristics of the system response include a rise time of 4.30 s, a settling time of 11.60 s, and a relatively smooth response without significant oscillations. Overshoot and steady-state error were calculated using Equations (16) and (17) based on the maximum response and steady-state values obtained from the experimental results. In the 100 cm setpoint test, a maximum response of 102 cm and a steady-state value of 100.36 cm were obtained, resulting in an overshoot of 2% and a steady-state error of 0.36%. These results indicate that the fine-tuned PID controller is capable of bringing the AUV to a depth of 100 cm with small overshoot and a final value very close to the setpoint. Therefore, the PID parameters used are considered effective for setpoint tracking and suitable for prototype AUV operation at a depth of 100 cm.

## 4. CONCLUSION

In this study, a PID-based depth control system for a prototype-scale autonomous underwater vehicle (AUV) was developed and experimentally validated using depth feedback from a SEN0257 pressure sensor. To improve measurement reliability, the sensor data were processed using a combination of a Kalman filter and a moving average filter and subsequently calibrated using a linear regression method. The calibration results demonstrate a significant improvement in depth estimation accuracy, with the RMSE value reduced from 1.88 cm to 0.63 cm. These findings confirm that a low-cost pressure sensor, when supported by appropriate filtering and calibration, can provide sufficiently accurate and stable depth feedback for closed-loop depth control in prototype AUV applications.

The control system performance was evaluated through an experimental comparison of two PID tuning methods, namely the Ziegler–Nichols method and manual fine-tuning, under both static conditions and forward motion maneuvers. At a depth setpoint of 70 cm, the fine-tuned PID controller exhibited a more stable response with smaller overshoot and lower steady-state error, although it showed a slightly slower rise time compared to the Ziegler–Nichols controller, which produced a faster but more aggressive response. Similar trends were observed during forward-motion tests, where the fine-tuned controller maintained smoother depth regulation with a shorter settling time. Furthermore, experiments conducted at a deeper setpoint of 100 cm demonstrated that the fine-tuned PID parameters remained effective and consistent despite changes in the reference depth.

Overall, this study provides experimental evidence that combining calibrated pressure-based depth estimation with practical PID fine-tuning significantly improves depth stability and control accuracy in prototype AUV systems. This contribution highlights the effectiveness of integrating low-cost sensing, signal processing, and control strategies under realistic operating conditions, thereby addressing the limited availability of experimental validation in existing studies.

## FUNDING INFORMATION

This research was supported by Politeknik Negeri Batam through internal research funding under the 2025 Research Grant Scheme.

## AUTHOR CONTRIBUTIONS STATEMENT

This study employs the Contributor Roles Taxonomy (CRediT) to acknowledge individual author contributions, mitigate authorship conflicts, and enhance collaboration.

| Name of Author | C | M | So | Va | Fo | I | R | D | O | E | Vi | Su | P | Fu |
|---|---|---|---|---|---|---|---|---|---|---|---|---|---|---|
| Senanjung Prayoga | ✓ | ✓ | | ✓ | ✓ | ✓ | ✓ | ✓ | | | | ✓ | ✓ | ✓ |
| Dhaniel Beny Wardhana | | | ✓ | ✓ | ✓ | ✓ | ✓ | ✓ | ✓ | | ✓ | | | |
| Ryan Satria Wijaya | ✓ | ✓ | | ✓ | ✓ | ✓ | ✓ | ✓ | | ✓ | ✓ | ✓ | | ✓ |

C : **C**onceptualization
M : **M**ethodology
So : **So**ftware
Va : **Va**lidation
Fo : **Fo**rmal analysis
I : **I**nvestigation
R : **R**esources
D : **D**ata Curation
O : Writing - **O**riginal Draft
E : Writing - Review & **E**diting
Vi : **Vi**sualization
Su : **Su**pervision
P : **P**roject administration
Fu : **Fu**nding acquisition

## CONFLICT OF INTEREST STATEMENT

The authors declare that there is no conflict of interest regarding the publication of this paper.

## DATA AVAILABILITY

The authors confirm that the data supporting the findings of this study are available within the article and its supplementary materials.

## REFERENCES

[1] C. Alexandris, P. Papageorgas, and D. Piromalis, "Positioning Systems for Unmanned Underwater Vehicles: A Comprehensive Review," Applied Sciences, vol. 14, no. 21, art. 9671, 2024, doi: 10.3390/app14219671.

[2] A. Bi, F. Zhao, X. Zhang, and T. Ge, "Combined Depth Control Strategy for Low-Speed and Long-Range Autonomous Underwater Vehicles," Journal of Marine Science and Engineering, vol. 8, no. 3, 181, 2020, doi: 10.3390/jmse8030181.

[3] X. Hu, Y. Li, Y. Meng, Y. Wang, and S. Wang, "A Highly Sensitive Deep-Sea Hydrodynamic Pressure Sensor for Long-Range AUVs," Photonics, vol. 9, no. 3, 190, 2024, doi: 10.3390/photonics9030190.

[4] Y. Sun, P. Chai, G. Zhang, T. Zhou, and H. Zheng, "Sliding Mode Motion Control for AUV with Dual-Observer Considering Thruster Uncertainty," Journal of Marine Science and Engineering, vol. 10, no. 3, 349, 2022, doi: 10.3390/jmse10030349.

[5] Z. Bingül and K. Gül, "Intelligent-PID with PD Feedforward Trajectory Tracking Control of an Autonomous Underwater Vehicle," Machines, vol. 11, no. 2, 300, 2023, doi: 10.3390/machines11020300.

[6] M. Przybylski, R. Piotrowski, J. Michalski, and P. Sala, "Selection of the Depth Controller for the Biomimetic Underwater Vehicle Drives," Electronics, vol. 12, no. 6, 1469, 2023, doi: 10.3390/electronics12061469.

[7] J. F. Carneiro, P. Branco, A. S. Martins, and P. M. Oliveira, "Depth Control of an Underwater Sensor Platform: Comparison Between Variable Buoyancy and Propeller-Actuated Devices," Sensors, vol. 24, no. 10, 3050, 2024, doi: 10.3390/s24103050.

[8] D. B. Duraibabu et al., “An Optical Fibre Depth (Pressure) Sensor for Remote Operated Vehicles in Underwater Applications,” Sensors, vol. 17, no. 2, p. 406, 2017, doi: 10.3390/s17020406.
[9] C.-L. Kuo et al., “Position Tracking of an Underwater Robot Based on Floating-Downing PI Control,” Processes, vol. 10, no. 11, p. 2346, 2022, doi: 10.3390/pr10112346.
[10] Blue Robotics, “T200 Thruster,” product page & specs, accessed Dec. 22, 2025.
[11] OpenStax, College Physics 2e, “Variation of Pressure with Depth in a Fluid (Hydrostatic Pressure P=ρghP=\rho ghP=ρgh),” accessed Dec. 22, 2025.
[12] DFRobot, “Gravity: Water Pressure Sensor (SEN0257) Datasheet (0.5–4.5 V linear output),” accessed Dec. 22, 2025.
[13] R. E. Kalman, “A New Approach to Linear Filtering and Prediction Problems,” Journal of Basic Engineering (ASME), vol. 82, no. 1, pp. 35–45, 1960, doi: 10.1115/1.3662552.
[14] S. W. Smith, The Scientist and Engineer’s Guide to Digital Signal Processing, Ch. 15 “Moving Average Filters,” Analog Devices, accessed Dec. 22, 2025.
[15] STMicroelectronics, “STM32F103x8/STM32F103xB Datasheet,” accessed Dec. 22, 2025.
[16] X. Liang et al., “An enhanced adaptive ensemble Kalman filter for autonomous underwater vehicle integrated navigation,” Drones, vol. 8, no. 12, art. 711, 2024, doi: 10.3390/drones8120711.
[17] Q. Xia et al., “Research on the depth control strategy of an underwater profiler driven by a mixture of ocean thermal energy and electric energy,” J. Mar. Sci. Eng., vol. 10, no. 5, art. 640, 2022, doi: 10.3390/jmse10050640.
[18] F. Dursun, S. Bilgin, N. N. Akkaya, “Depth Control Based on PID Using a Pressure Sensor in an Autonomous Underwater Vehicle,” ELECO 2025 (Proc.), 2025.
[19] A. Hermansyah, W. H. Purnomo, I. M. D. P. Asana, “PID Implementation for Depth Control and Navigation of Underwater Robots,” JEEE-U, vol. 9, no. 1, 2025.
[20] J. Sanjaya, A. J. Setiawan, G. Santoso, “Performance Analysis of PID and SMC Control Algorithms for AUV Depth Controller Using EKF Sensor Fusion,” Jurnal Riset Teknologi dan Inovasi Pendidikan (SPIR), 2024.
[21] H. N. Tran, T. N. N. Pham, S. H. Choi, “Robust depth control of a hybrid autonomous underwater vehicle with propeller torque’s effect and model uncertainty,” Ocean Engineering, 2021.
[22] M. Huba, “Making the PI and PID Controller Tuning Inspired by Ziegler and Nichols Precise and Reliable,” Sensors, 2021.
[23] Ł. Lemieszewski and P. Puzio, “Optimization of PID Controller Settings Using the Ziegler–Nichols Method in Pneumatic Pressure Control Systems,” Procedia Computer Science, vol. 270, pp. 5177–5186, 2025, doi: 10.1016/j.procs.2025.09.645.
[24] R. S. Patil, S. P. Jadhav, and M. D. Patil, "Review of Intelligent and Nature-Inspired Algorithms-Based Methods for Tuning PID Controllers in Industrial Applications," Journal of Robotics and Control, vol. 5, no. 2, pp. 336–358, Mar. 2024, doi: 10.18196/jrc.v5i2.20850.
[25] P. J. W. Widodo, H. Sukanto, B. Santoso, F. Imaduddin, L. L. G. Hidayat, J. Triyono, I. Istanto, and R. Wijaya, "A Comparative Study of Traditional PID Tuning Techniques and AI-Based Algorithmic Approaches Utilizing the Python Control Library," Jurnal Ecotipe, vol. 12, no. 2, pp. 234–244, Oct. 2025, doi: 10.33019/jurnalecotipe.v12i2.4574.
[26] H. Supriyanto et al., “Implementasi kontroler PID dengan metode tuning Ziegler-Nichols dan Cohen-Coon,” Jurnal Teknologi Terapan (Polindra), 2022.


## BIOGRAPHIES OF AUTHORS

**Senanjung Prayoga** received the M.T. degree in Engineering Physics. He is currently serving as a Lecturer (Assistant Professor) with the Department of Robotics Engineering Technology, Politeknik Negeri Batam, Batam, Indonesia. He has served as an advisor for competitive robotics teams, including wheeled soccer robots and legged search-and-rescue (SAR) robots. He is currently developing a mobile robot platform intended for educational purposes. His research interests include mobile robotics, control systems, numerical methods, path planning, and simultaneous localization and mapping (SLAM).

**Dhaniel Beny Wardhana** Dhaniel Beny Wardhana is an undergraduate student in Robotics Engineering at Politeknik Negeri Batam. His technical interests include sensor fusion, motion control, robotic electrical system, machine learning, and embedded system. During his studies, he has actively developed applied projects that integrate data processing, programming, and end-to-end system implementation. His research experience focuses on the development of Autonomous Underwater Vehicle (AUV), particularly in designing and implementing control system to support navigation and motion stability. He has also participated in robotics competitions such as the Indonesian Underwater Robotics Contest (KRBAI) and the Singapore Autonomous Underwater Vehicle Challenge (SAUVC), which strengthened his skills in hardware-software integration, experimental testing, and iterative performance improvement. In addition. He contributed to the design of a hockey-playing robot as a platform to enhance system engineering skills and design iteration. In this study, he contributed to the research methodology, data analysis, and system implementation, supporting both the technical development and the performance evaluation of the proposed approach.

**Ryan Satria Wijaya** Assistant Professor, a lecturer at Politeknik Negeri Batam specializing in Robotics, Motion Control, Computer Vision, and Artificial Intelligence, has contributed to various research projects and publications in these fields. His work includes studies on deep learning algorithms for object detection, path planning in service robots, and the development of interactive learning media for vocational education. His research aims to advance technological applications in robotics and AI, enhancing both academic understanding and practical implementations.